Chemistry and Physics of Lipids 165 (2012) 89–96

Contents lists available at SciVerse ScienceDirect

Chemistry and Physics of Lipids

journal homepage: www.elsevier.com/locate/chemphyslip

# Oligoarginine vectors for intracellular delivery: Role of arginine side-chain orientation in chain length-dependent destabilization of lipid membranes

A.M. Bouchet[a,b], F. Lairion[b,*], J.-M. Ruysschaert[a], M.F. Lensink[c]

[a] Structure and Function of Biological Membranes, Université Libre de Bruxelles, Boulevard du Triomphe – CP 206/2, B-1050 Brussels, Belgium
[b] Laboratorio de Fisicoquimica de Membranas Lipidicas, Facultad de Farmacia y Bioquimica, U. B. A. Junin 956 2°P, (1113) Buenos Aires, Argentina
[c] Biological Nanosystems, Interdisciplinary Research Institute, University of Sciences and Technology Lille, USR3078 CNRS, 50 Avenue Halley, F-59658 Villeneuve d'Ascq, France

ARTICLE INFO

*Article history:*
Received 6 October 2011
Received in revised form
11 November 2011
Accepted 12 November 2011
Available online 19 November 2011

*Keywords:*
Oligoarginine
Bilayer destabilization
ATR-FTIR
Lipids
Cell-penetrating peptide
Molecular dynamics

ABSTRACT

Arginine-rich peptides receive increased attention due to their capacity to cross different types of membranes and to transport cargo molecules inside cells. Even though peptide-induced destabilization has been investigated extensively, little is known about the peptide side-chain and backbone orientation with respect to the bilayer that may contribute to a molecular understanding of the peptide-induced membrane perturbations.

The main objective of this work is to provide a detailed description of the orientation of arginine peptides in the lipid bilayer of PC and negatively charged PG liposomes using ATR-IR spectroscopy and molecular modeling, and to relate these orientational preferences to lipid bilayer destabilization.

Molecular modeling showed that above the transition temperature arginine side-chains are preferentially solvent-directed at the PC/water interface whereas several arginine side-chains are pointing towards the PG hydrophobic core. IR dichroic spectra confirmed the orientation of the arginine side chains perpendicular to the lipid–water interface. IR spectra shows an randomly distributed backbone that seems essential to optimize interactions with the lipid membrane. The observed increase of permeation to a fluorescent dye is related to the peptide induced-formation of gauche bonds in the acyl chains. In the absence of hydrophobic residues, insertion of side-chains that favors phosphate/guanidium interaction is another mechanism of membrane permeabilization that has not been further analyzed so far.

© 2011 Elsevier Ireland Ltd. All rights reserved.

## 1. Introduction

Cell penetrating peptides (CPPs) display the ability to cross cell membranes and transport cargo molecules inside cells. One of the most representative members of this family of peptides is a short, arginine-rich peptide segment derived from the human immunodeficiency virus (HIV)-1Tat protein. Cellular uptake mechanisms remain nevertheless controversial. For instance, it has been suggested that the TAT peptide translocates with its cargo into eukaryotic cells through a physical mechanism that is not receptor-mediated, without implicating the endosomal pathway (Henriques et al., 2005). This suggests that translocation would require a rearrangement of the lipid bilayer organization and/or packing. In contrast, other studies propose a raft-dependent endocytic pathway, involving macropinocytosis (Wadia et al., 2004). These membrane-permeable peptides share little similarity in their primary and secondary structures except for a high concentration of arginine residues in their sequences. In addition, various arginine-rich oligopeptides display very similar properties in terms of translocation and delivery efficiency, suggesting an obvious correlation between translocation and arginine content (Futaki, 2006). The translocation may be a consequence of the interaction between the hydrophilic moiety of phospholipids and the side-chains of arginine residues as suggested by the arginine-rich peptides' length-dependent internalization and the absence of internalization of peptides with three arginine residues or less (Tung and Weissleder, 2003).

Whereas part of CPPs uptake might involve specific receptors, internalization is observed even in their absence (Richard et al., 2005). Furthermore, these peptides can enter giant unilamellar vesicles made exclusively of lipids (Binder and Lindblom, 2003). All together these data strongly suggest that a specific interaction between the hydrophilic moiety of phospholipids and the side-chains of arginine residues is an important step for peptide internalization.

The interaction between the CPPs and the cell membrane is the first step involved in the uptake mechanism. Even though peptide-induced membrane perturbations has been investigated

* Corresponding author. Tel.: +54 1149648249.
*E-mail address:* flairion@ffyb.uba.ar (F. Lairion).

0009-3084/$ – see front matter © 2011 Elsevier Ireland Ltd. All rights reserved.
doi:10.1016/j.chemphyslip.2011.11.008

extensively, little information is available about the orientation of the peptide side-chains and backbone with respect to the bilayer that may open the way to a molecular understanding of the peptide-induced membrane perturbations. The fact that the hydrophobic residues present in the sequence of these penetrating peptides favored penetration is possibly a direct consequence of an increased hydrophobicity. The challenge of this work is to deal with highly hydrophilic peptide and to understand how it could nevertheless destabilize a lipid bilayer. Therefore, the main objective of this work is to provide a description of the backbone and side-chain orientation of Arginine oligopeptides (Arg4, Arg7) in the lipid bilayer, in comparison with the isolated amino acid (arg+), using ATR-IR spectroscopy and molecular dynamics simulation and to relate orientation preferences of the peptide with the lipid bilayer packing and organization. In this sense we use zwitterionic PC and negatively charged PG because we want to reveal the mechanism of binding which always precedes a possible translocation, focusing on the influence that peptide binding has on lipid membrane properties. The phosphate moiety was identified in previous studies as a prominent factor in arginine–lipid interaction and therefore DMPG appeared as a valuable biophysical model (Sakai et al., 2005; Tang et al., 2007).

## 2. Materials

DMPC, DMPG, DOPG were purchased from Avanti Polar Lipids, Inc. (Alabaster, AL) and used as received. Peptides and amino-acids: Arg7, Arg4 were from AnyGen Co. Ltd., and L-arginine (arg+) was obtained from Sigma–Aldrich (Saint Louis, MO).

### 2.1. Preparation of liposomes

Lipids were dissolved in chloroform:methanol mixture (3:1 ratio), evaporated under nitrogen flow and desiccated overnight under vacuum to remove any residual solvent. Dried films were vortexed at 40 °C in Tris:NaCl buffer 10:100 mM (pH 7.3).

## 3. Methods

### 3.1. Attenuated total reflection Fourier transform IR spectroscopy (ATR-FTIR)

The internal reflection element was a 52 mm × 20 mm × 2 mm trapezoidal germanium ATR plate with an aperture angle of 45° yielding 25 internal reflections. Infra-red spectra were recorded on an IFS55 FTIR spectrophotometer (Bruker, Ettlingen, Germany) purged with $N_2$. Fifteen microliters of the liposomes sample were deposited under a stream of nitrogen on one side of the germanium. While evaporating, capillary forces flattened the membranes which spontaneously formed oriented multilayer arrangements. Under these conditions a well ordered multilayer stack is formed (Vigano et al., 2000a) it remains stable under a buffer flow (Scheirlinckx et al., 2004). The peptides were added to the lipids at several molar ratios. Spectra were recorded with 2 $cm^{-1}$ spectral resolution between 4000 and 800 $cm^{-1}$ with a broad-band MCT detector provided by Bruker; 128 scans were averaged for one spectrum at each temperature analyzed. A modified continuous flow ATR setup was equipped with a polarizer that can be oriented parallel or perpendicular to the incidence plane. An elevator under computer control made it possible to move the whole setup along a vertical axis. This allowed the crystal to be separated in different lanes. Here, one lane contained the membrane film and the other was used for the background. All spectra were corrected for water vapor contribution and $CO_2$ and finally apodized at a resolution of 4 $cm^{-1}$. All the software used for data processing was written under MatLab 7.0 (Mathworks Inc., Natick, MA).

### 3.2. Lipid bilayer acyl chain conformations

IR spectra were recorded with and without peptides in the 3000–2800 $cm^{-1}$ range, to monitor the lipid state of order and the motional freedom of the methyl groups (Casal and Mantsch, 1984).

### 3.3. Secondary structure evaluation

DMPC and DMPG liposomes were spread on the diamond crystal and dried under $N_2$ flow. The peptide film was incubated with arginine peptides of different length and washed with water to remove unbounded peptide. The sample was rehydrated by flushing $D_2O$-saturated $N_2$ for 2 h at room temperature. 512 Scans were averaged for each measurement. The determination of the secondary structure was based on the shape of the amide I band (1600–1700 $cm^{-1}$), which is sensitive to the secondary structure. The analysis was performed on the amide I region of deuterated samples in order to differentiate the α-helical secondary structure from the random secondary structure whose absorption band shifts from about 1655 $cm^{-1}$ to about 1642 $cm^{-1}$ (Goormaghtigh et al., 2006; Oberg et al., 2004; Vigano et al., 2000b).

### 3.4. Secondary structure orientation

The orientation of different secondary structures was determined as described previously (Bechinger et al., 1999; Grimard et al., 2001). Spectra were recorded with the incident light polarized parallel and perpendicular with respect to the incidence plane. Dichroic spectra were computed by subtracting the perpendicular polarized spectrum from the parallel polarized spectrum. The subtraction coefficient was chosen such that the area of the lipid ester band at 1740 $cm^{-1}$ equaled zero on the dichroism spectrum, in order to take into account the difference in the relative power of the evanescent field for each polarization and also the differences in film thickness as described previously.

An upward deviation on the dichroism spectrum indicates a dipole oriented preferentially near the normal to the ATR plate. Conversely, a downward deviation on the dichroism spectrum indicates a dipole oriented parallel to the plane of the ATR plate.

### 3.5. Molecular dynamics simulations

MD simulations have been performed with the Gromacs 3.3.1 package (Van Der Spoel et al., 2005) using the Gromos96 43a2 force field (van Gunsteren, 1996) extended with lipid head group (Lensink et al., 2005) and acyl chain parameters (van Gunsteren, 1996). An equilibrated bilayer of 128 POPC molecules was taken as the starting point (Tieleman et al., 1999). From this bilayer a POPG bilayer was created using the same procedure as before (Lensink et al., 2005). An arginine oligomer (Arg7) was initially placed at a distance of 2 nm from the bilayer surface. Various initial conformations were explored (extended, α-helical, β-turn), but found to all converge to a similar unordered structure during and after association with the bilayer. Single point charge water was used (Berendsen et al., 1981). The systems were made electrostatically neutral by adding the required amount of counterions $Na^+$ or $Cl^-$ and then submitted to an energy minimization and 10 ps MD with position restraints on the peptide heavy atoms and lipid tail atoms. Weak coupling to a temperature (310 K, separate coupling for peptide, lipids and solvent including ions) and pressure (anisotropic, 1.0 bar) bath was employed (Berendsen et al., 1984) using coupling constants of 0.1 and 1.0 ps, resp. Coulomb interactions were treated

with fast particle mesh Ewald, a grid spacing of 0.12 nm and fourth-order interpolation was employed (Essman et al., 1995). A cut-off distance of 1.0 nm was applied to the Van der Waals interactions. Bond lengths were constrained using the LINCS algorithm (Hess et al., 1997). Equations of motion for the water atoms were solved analytically with the SETTLE algorithm (Miyamoto and Kollman, 1992). Dummy atoms were used to limit high-frequency vibrations involving hydrogen atoms (Feenstra et al., 1999). A time step of 4 fs was employed, removing center of mass motion every step and updating the neighbor list every 5 steps. As we were also interested in the association with the lipid bilayer, analyses were performed over the entire simulation lengths of 100 ns, unless stated otherwise. Lipids are defined as interacting with the peptide when any of their atoms are within a cylinder, parallel to the bilayer normal ($z$-axis), with diameter 0.1 nm and height 1 nm from any of the peptide atoms, as before (Lensink et al., 2005).

### 3.6. Leakage experiments

4 mg of lipid was vortexed with 2 ml of 20 mM carboxyfluorescein (pH 7) above the main lipid transition temperature. Large unilamellar vesicles (LUVs) were prepared by extrusion through two polycarbonate membranes with a pore size of 100 nm (Avanti Polar Lipids, Inc., Alabaster, AL, USA). The extrusion temperature was maintained 10 °C above the phase transition temperature ($T_m$). Non-entrapped carboxyfluorescein was removed on a Sephadex G-75 column.

Lipid content was determined by phosphate determination assays (Rouser et al., 1966). Peptide induced vesicular leakage was evaluated by monitoring the fluorescence intensity increase recorded at 517 nm (excitation 490 nm).

Percentage of leakage was calculated as: $100(I - I_0)/(I_d - I_0)$, where $I_0$ is the initial fluorescence intensity, $I$ the recorded fluorescence intensity and $I_d$ is the intensity after addition of Triton X-100 (to 0.1%, v/v).

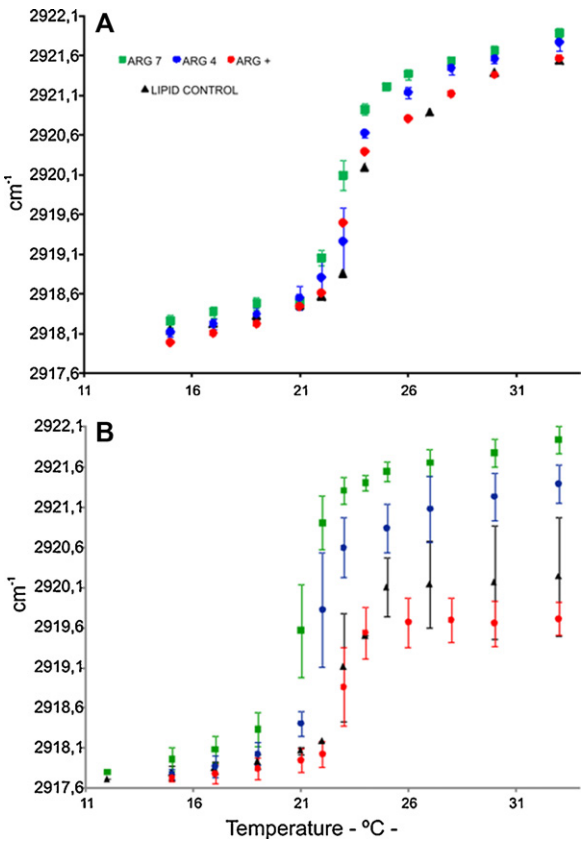


**Fig. 1.** Evolution of the maximum frequency of the asymmetric $CH_2$ stretching vibration (2929 $cm^{-1}$), as a function of temperature for DMPC (A) and DMPG (B) in the presence of peptides Arg7, Arg4 and arg+. The concentration of phospholipids is 10 mg/ml. The lipid:peptide molar ratio is 1:2 and the lipid:amino-acids ratio is 1:450.

## 4. Results

### 4.1. Arginine-induced lipid bilayer perturbations

#### 4.1.1. ATR-IR

The transition from gel to liquid crystalline phase causes conformational disorders in the acyl chains (i.e., *gauche* rotamers) and rearrangements in the interfacial and polar head group regions, leading to major changes in the infrared spectrum. IR bands in the 3000–2800 $cm^{-1}$ region arise predominantly from the symmetrical and asymmetrical $CH_2$ and $CH_3$ stretching vibrations and are quite sensitive to temperature-induced changes. The frequency, the intensity, and the width of these bands specifically monitor the membrane state of order and the motional freedom of the methylene groups (Casal and Mantsch, 1984).

In order to accurately determine the peak maxima, a Gaussian curve was fitted onto the upper half of the position of the maximum of the asymmetric $CH_2$ stretching vibrations of DMPC and DMPG vesicles and the result was plotted as a function of temperature (Fig. 1A and B). A drastic change of the maximum frequency of the $CH_2$ asymmetric vibration is observed at the phase transition temperature of the pure lipid (23 °C for DMPC), revealing a significant increase of gauche rotamers. This pattern is not significantly modified in the presence of arg+ or Arg4 (Fig. 1A), even at high peptide/lipid molar ratios. No shift of the transition temperature was detected.

In contrast, addition of Arg4 and Arg7 to anionic DMPG vesicles induced a significant change in the shape of the melting curve and the transition temperature (Fig. 1B). Again a drastic change of the $CH_2$ asymmetric vibration is observed around 23 °C, revealing a significant increase of gauche rotamers around the transition temperature. An identical shift is observed for the $CH_2$ symmetric vibration (data not shown). A minor increase of absorbance of $\nu_{as}(CH_2)$ stretching is observed below the transition temperature after addition of Arg4 and Arg7. Above the transition temperature, at 37 °C Arg does not affect the frequency of pure DMPG within the experimental error and Arg 4 and Arg7 increases in that order the frequency difference.

#### 4.1.2. Arginine-induced leakage of carboxyfluorescein encapsulated into phospholipids vesicles

Self-quenching of a fluorescent dye (carboxyfluorescein) encapsulated in the inner aqueous phase of unilamellar vesicles was used as a measure of the dye release resulting from the peptide interaction with the lipid membrane. At temperature at which the bilayers were at the liquid crystalline state (37 °C), arg+ does not promote carboxyfluorescein leakage from DMPC vesicles but a slight but significant leakage is observed with Arg4 and 7 (Fig. 2). Arg and Arg4 cause a small leakage in DMPG but Arg7 a drastic one.

The asymmetric $CH_2$ stretching vibration at 37 °C (Fig. 1) for DMPC and DMPG and the extent of leakages follows the same sequence arg+ < Arg4 < Arg 7. The changes in peptide/lipid ratio increases the percentage of leakage, being maximal at a 3:1 lipid:peptide molar ratio (Fig. 3).

It is likely that graded leakage is caused by short-lived membrane defects distributed over the lipid membrane and due to the asymmetric insertion of the peptide into the outer leaflet. It is based in the bilayers-couple model which describes the effect of

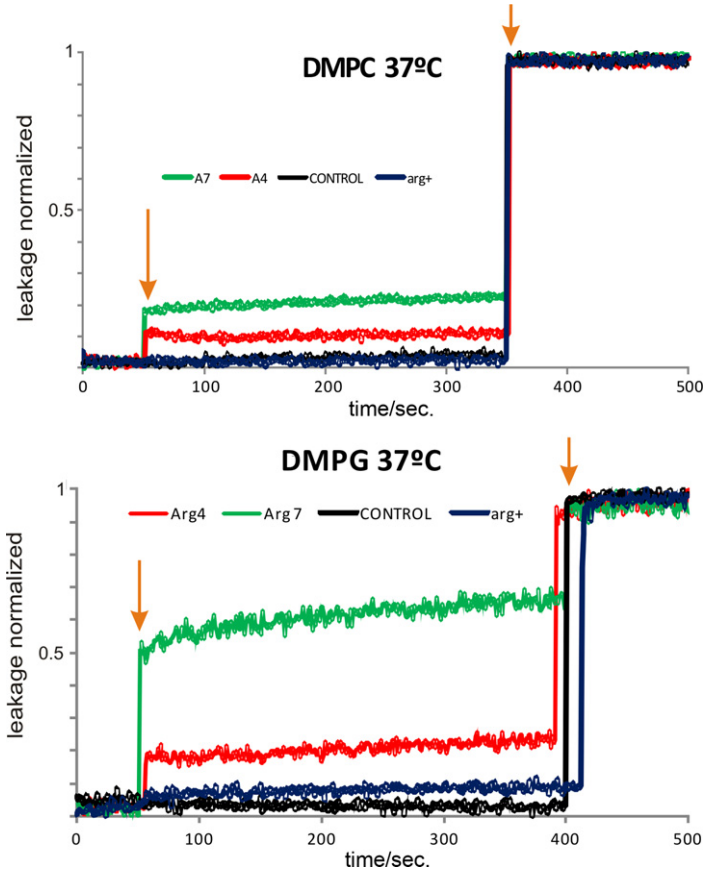


**Fig. 2.** Percentage of leakage normalized as a function of time, for DMPC and DMPG at 37 °C in the presence of peptides Arg7, Arg4 and arg+. The lipid:peptide molar ratio is 1:2 and the lipid:amino-acids ratio is 1:450. The orange arrow indicates the addition of peptide and Triton respectively.

destabilizing molecules that cannot flip quickly from the outer to the inner monolayer (Heerklotz and Seelig, 2007). Their insertion into the auter monolayer leads to an asymmetric increase in lateral pressure that tends to bend the bilayers and may lead to a transient disruption of the membrane at a certain threshold. The relative distribution of peptide between the inner and the outer leaflet can be estimated from an evaluation of the surface charge density in the absence of peptide and with peptide located on the internal and external surface. Measurements of the zeta potentials carried out in the absence and presence of peptides revealed that most of arg7 is located on the outer monolayer (Bouchet, A., Lairion, F., Disalvo, A., unpublished data).

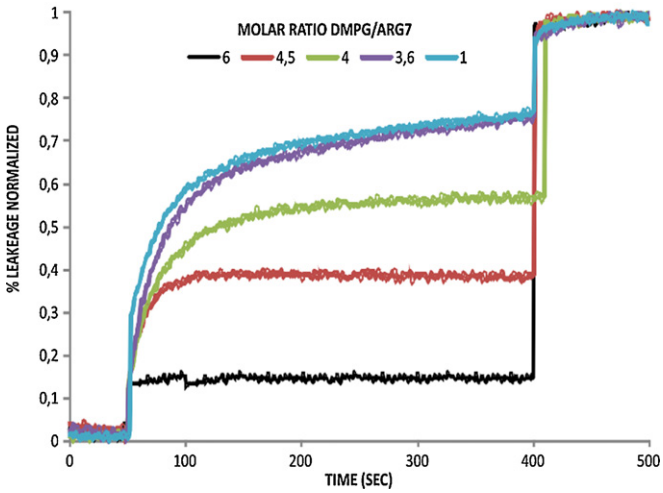


**Fig. 3.** Percentage of leakage normalized as a function of time of DMPG vesicles at different concentration of Arg7 at 37 °C, added at 50 s.

### 4.2. Structure and orientation of Arginine oligomers interacting with DMPC and DMPG bilayers

#### 4.2.1. Secondary structure evaluation in the presence of DMPG

Deconvolution and curve fit reveal major contributions at 1673 and 1633 $cm^{-1}$ for Arg7/DMPG in $H_2O$ and at 1608 and 1586 $cm^{-1}$ in $D_2O$, corresponding to the asymmetric and symmetric arginine side-chains (Venyaminov and Kalnin, 1990; Wolpert and Hellwig, 2006). Spectral analysis was performed in the amide I region of deuterated samples since H/D exchange allows to differentiate the α-helical from the random secondary structure. The absorption shift from about 1651–1655 $cm^{-1}$ in water to about 1644–1646 $cm^{-1}$ in $D_2O$ regardless of peptide chain length, is indicative of a backbone adopting a random structure (see also Fig. 4 and Table 1).

**Table 1**
Analysis of AMIDE I in terms of secondary structure for Arg7 and Arg4, in water and deuterated water.

| | $H_2O$ ($cm^{-1}$) | $D_2O$ ($cm^{-1}$) |
|---|---|---|
| Arg4 | 1651 | 1644 |
| Arg7 | 1656 | 1646 |

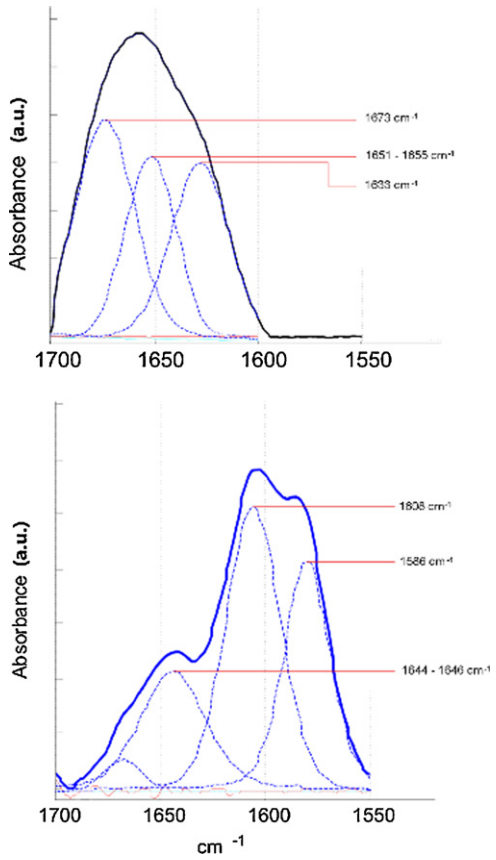


**Fig. 4.** ATR-FTIR spectra of DMPG at 21 °C, in the presence of Arg7, in water (black above) and in deuterated water (blue below). Deconvolution reveal peaks (1651–1655 $cm^{-1}$ in water to about 1644–1646 $cm^{-1}$ in $D_2O$) that can be assigned to the peptide backbone. Deconvolution and curve fitting reveal major contributions at 1673 and 1633 $cm^{-1}$ for Arg7/DMPG in $H_2O$ and at 1608 and 1586 $cm^{-1}$ in $D_2O$, corresponding to the asymmetric and symmetric arginine side-chains. (For interpretation of the references to color in this figure legend, the reader is referred to the web version of the article.)

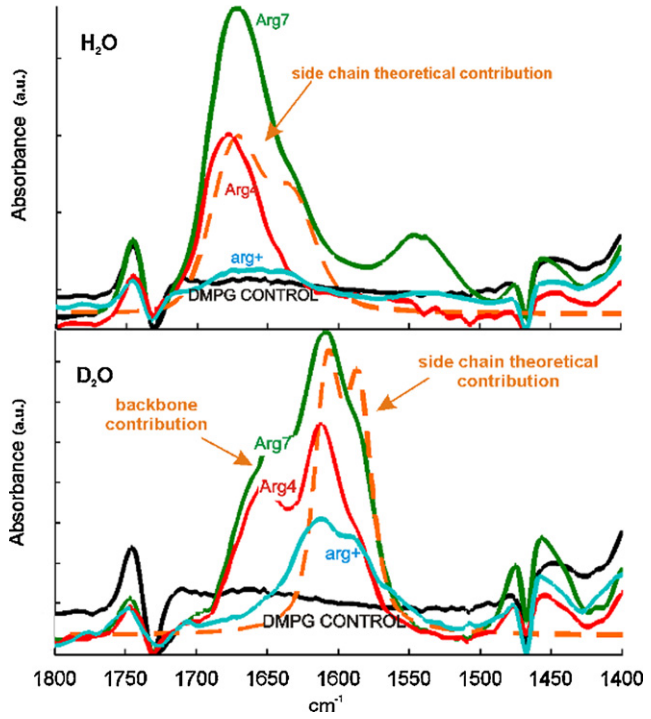


**Fig. 5.** Dichroic spectra of DMPG control (black) and after addition of Arg7 (green), Arg4 (red) and arg+ (light blue) at 21 °C. The main side-chain contribution (guanidinium group) is represented with dotted line. (For interpretation of the references to color in this figure legend, the reader is referred to the web version of the article.)

#### *4.2.2. Orientation in the lipid bilayers of secondary structure and side-chain of arginine peptides*

After incubation of arg+, Arg4 and Arg7 with DMPC liposomes, no change of dichroic signal was detected (data no shown) in the amide I region. In contrast, a major change of the dichroic spectra was observed at 1673 and 1633 $cm^{-1}$ in $H_2O$, and at 1608 and 1586 $cm^{-1}$ in $D_2O$, when Arg4 and Arg7 are incubated with DMPG liposomes (Fig. 5). As mentioned before, these two peaks correspond to the symmetric and asymmetric vibration of the arginine side-chains. The positive deviation observed for oligomers 4 and 7 are the signature of a preferential orientation of the transition dipoles of the arginine side-chains perpendicular to the lipid/water interface. On the other hand, the spectra do not reveal any dichroic signal associated with the protein backbone which is the signature of a non-oriented backbone.

### *4.3. Molecular dynamics simulations*

MD simulations have been performed to investigate the association of Arg7 with a bilayer consisting of POPC and of POPG lipids, based on the fact that the interaction parameters of MD for both lipids are more established than for DMPC and DMPG.

On average 15 lipids are found to interact with the peptide. This number is quickly reached, within the first few nanoseconds of the simulations, due to the fast association of the peptide with both bilayers. Fig. 6 shows the calculated deuterium order parameters for the sn1 and sn2 chains of the lipids. It can clearly be seen that the lipids that are interacting with the peptide are much more distorted in the case of POPG (bottom graphs) than in the case of POPC (top graphs). The sn1 chain is more affected than the sn2 chain.

A closer look at the conformation of the peptide reveals that if the overall secondary structure is quite similar in the two bilayers (see Fig. 7), the orientation is not. In Fig. 8 we have plotted the differential distance to the bilayer center. This distance is defined as the difference of the distance of the peptide backbone and side-chains atoms to the center of the bilayer, with a lower value indicating the side-chain atoms to be located closer to the bilayer center than the backbone atoms. The figure shows the side-chain atoms to be almost a full Ångstrøm closer to the center of the bilayer in the case of POPG. This is especially relevant since the bilayer width of POPG is larger than the one of POPC; calculated over the last 50 ns of the trajectories, the average phosphate-to-phosphate distance is 3.90 nm for the POPC bilayer and 4.47 nm for the POPG bilayer (Fig. 9).

This results in an image where the arginine side-chains are oriented towards the aqueous phase in the case of POPC, and towards the hydrophobic bilayer core in the case of POPG. We have plotted two representative frames of the simulations in Fig. 10(A and B). The left-hand panel shows the interaction of Arg7 with a POPC bilayer, the right-hand panel with a POPG bilayer. All observations that were made for the interaction with PG, more disordered lipids, increased bilayer destabilization, preferred side-chain orientation, are apparent in this picture and confirm the experimental data. From the image it can be seen that some lipid phosphorus groups are located underneath the peptide in the PG bilayer. When we look into the interactions between these phosphate groups and the arginine side-chains, we can calculate the radial distribution function of arginine side-chain nitrogen atoms around lipid phosphate oxygens, depicted in Fig. 9. The figure shows the (normalized) number of nitrogen atoms around any $PO_4$ oxygen. The first peak,

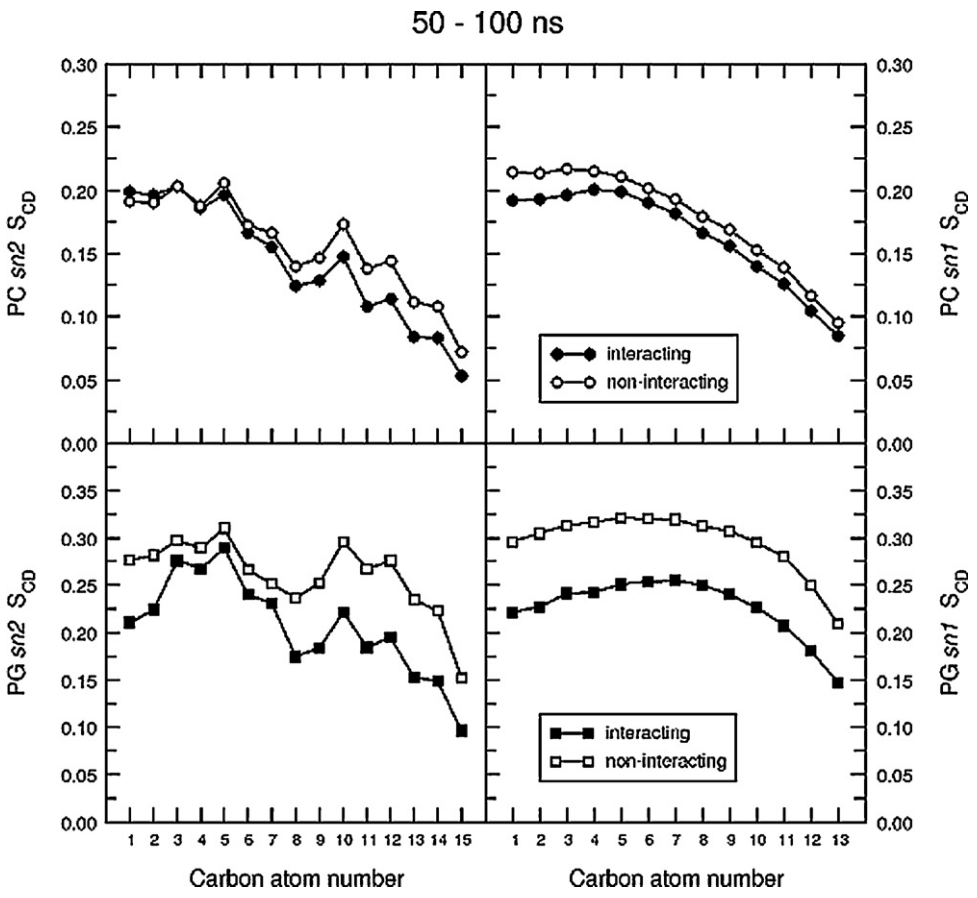


**Fig. 6.** Lipid acyl chain order parameters, calculated over the last 50 ns of the MD simulations for Arg7 interacting with a POPC (top panels) or POPG (bottom panels) bilayer. Left-hand panels show data for the sn2 oleoyl chain, right-hand panels for the sn1 palmitoyl chain. Closed points denote the order parameters for the lipids that are interacting with the peptide, open points denote the order parameters for the lipids that are not interacting with the peptide. Interaction is defined as in Section 2.

corresponding to a distance of 0.27 nm, is the strongest hydrogen bond (distance is donor to acceptor; subtract 0.1 nm for hydrogen to acceptor distance). The graph clearly shows a strongly increased interaction for the PG bilayer, over the entire plotted range. This interaction results from an increased number of arginine side-chains binding a PG phosphorus group. A typical interaction frame is shown in Fig. 11. The interaction shows R3 and R6 interacting with the lipid $PO_4$. Note that an additional $PO_4$ oxygen is available for interaction with R5. This interaction can still be formed by Arg4, but not by arg+.

## 5. Discussion

Comparison of different backbones showed that a main requirement for cellular uptake is an unordered backbone; this parameter seems essential to optimize interactions with the lipid membrane. The absorption band shift from about 1651–1655 $cm^{-1}$ to about 1644–1646 $cm^{-1}$, regardless of the chain length of the peptide, is indicative of a backbone adopting a random structure and confirms these assumptions. The fact that no leakage is observed with free arginine indicates that even though electrostatic interactions are involved, a network generated by covalently bound arginines is a prerequisite for leakage. It is relevant to mention that experiments carried out with oligomers comprising all D- or all L-amino acids revealed a similar uptake, suggesting that the backbone is not critical (Mitchell et al., 2000). Even more, the replacement of the peptidic backbone was found to improve cellular uptake (Rothbard et al., 2002; Wender et al., 2002).

Even if the arginine peptide backbone does not penetrate deeply inside the lipid bilayer, molecular dynamics simulations suggest that the interaction of the arginine side-chain with the phosphate group of POPG brings them more inside the membrane, causing a local thinning of the membrane as suggested by the data in Fig. 8. It is likely that this effect is amplified by the clustering of

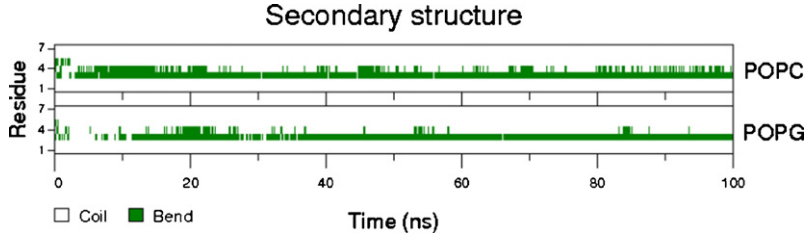


**Fig. 7.** Secondary structure evolution during the course of the simulations. In both bilayer systems (POPC and POPG), Arg7 is found to adopt an unordered structure, with only residue 3 (and 4 occasionally) answering the secondary structure criteria for 'Bend' (Kabsch and Sander, 1983).

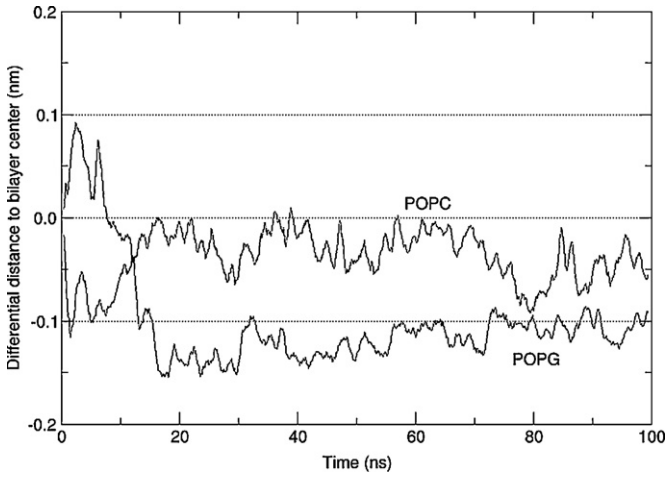


**Fig. 8.** Differential distance to the bilayer center, between the side-chain and backbone atoms of Arg7. A lower value indicates that the side-chain is closer to the center of the bilayer than the backbone.

several Arg7 peptides at the surface of the membrane. Although Arg7 promotes a slight increase in the $CH_2$ rotamers below the transition temperature, leakage is absent denoting that the number of gauche rotamers is not sufficient to induce measurable permeability changes.

The most prominent leakage is observed for Arg7 at 37 °C, above the DMPG transition temperature, where the increased mobility of the acyl chains allows the penetration of side-chains into the bilayer. At this temperature the effect of Arg7 on the conformational rotamers of $CH_2$ are higher than that promoted by Arg4 (Fig. 1).

Despite the fact that the MD simulations were performed with POPC and POPG instead of DMPC and DMPG, they show the arginine-peptides to remain in the head group area, which is invariant between simulation and experiments. We therefore do not expect significant differences. Molecular modeling showed that above the transition temperature arginine side-chains did not show any privileged orientation at the POPC water interface whereas several arginine side-chains are pointing towards the

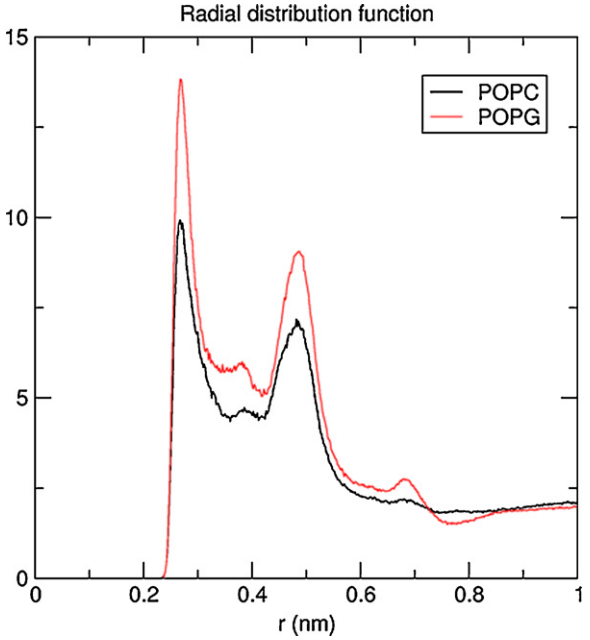


**Fig. 9.** Radial distribution function of Arg7 side-chain nitrogens to lipid (POPC: black; POPG: red) $PO_4$ oxygens.

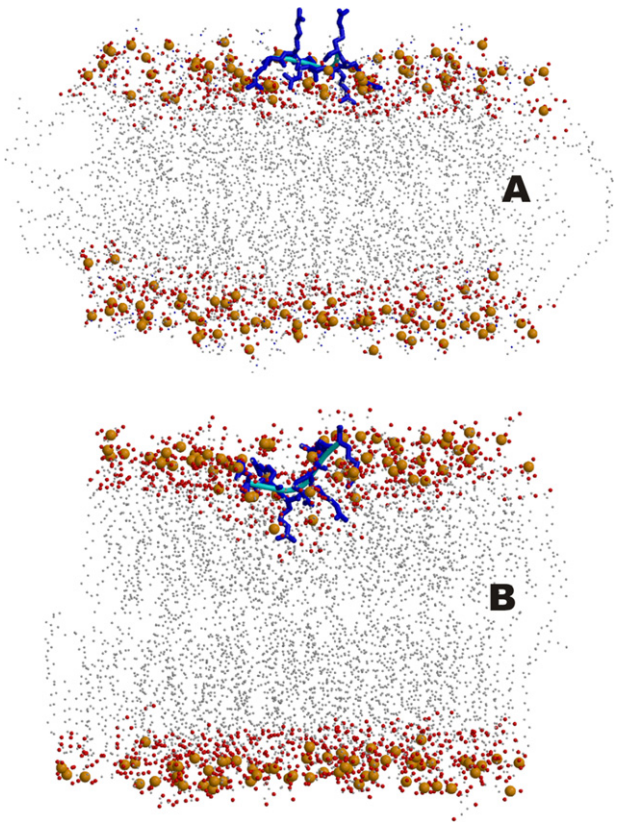


**Fig. 10.** Representative frame of Arg7 association with PC (A) and PG (B) bilayers. Arg7 drawn in blue wireframe, lipid atoms drawn as spheres, using large orange spheres for the phosphorus atoms, small red spheres for its liganding oxygens, and small gray spheres for the acyl tail carbons. Remaining lipid atoms and water are not shown for reasons of clarity. (For interpretation of the references to color in this figure legend, the reader is referred to the web version of the article.)

POPG hydrophobic core. The concentration of several phosphate residues around the arginine side-chains, as observed for POPG but not for POPC, suggests that the accessibility of the phosphate moieties is a crucial requirement for the penetration of arginine

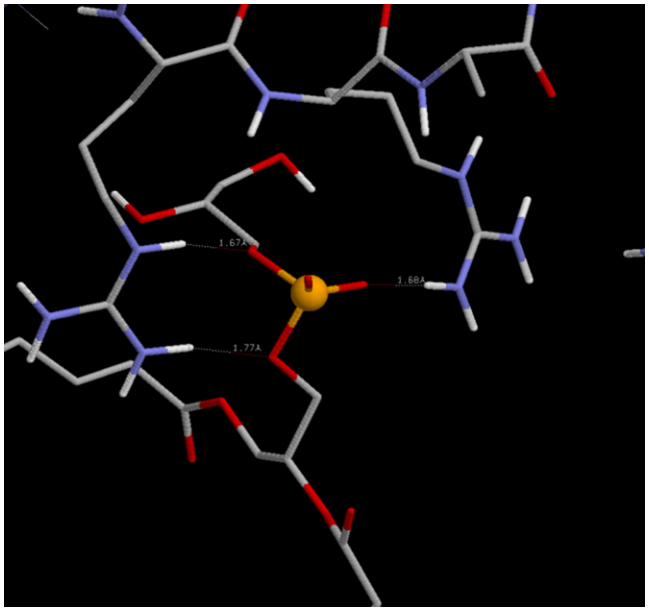

**Fig. 11.** Typical frame showing the liganding interaction of arginine side-chains around a PG phosphorus group.

side-chains, which was already reported to play a key role in arginine interaction with membrane lipids (Schwieger and Blume, 2009; Tang et al., 2007). It is likely that this penetration requires the formation of a dentate complex. Although such an interaction can also be formed with PC lipids, the electrostatic repulsion from the PC choline group effectively lowers the number of lipid $PO_4$-liganding arginines, as can be seen in Fig. 9.

This picture is in complete agreement with the dichroic spectra. Indeed, arginine side-chains are oriented normal with respect to the DMPG bilayer and do not show any privileged orientation in DMPC bilayers.

Whether and how the positively charged arginine can insert into the hydrophobic core of the lipid membrane is still a matter of debate. It has been proposed, based on computer simulations that the transfer of arginine through the hydrocarbon core of a lipid bilayer requires the formation of water-filled defect that keep arginine molecules hydrated (MacCallum et al., 2008, 2011). Another possibility is the formation of a hydrogen-bonded network made of water and lipid phosphates, formed around the arginine residues that might lead to the formation of a voltage-gated channel. This interaction reduced the hydrocarbon bilayer thickness to 10 Å (Freites et al., 2005) but at this stage we do not have experimental arguments to validate such a model.

Most peptides that destabilize the bilayer adopt an organized structure (helix or beta-sheet), which favors the orientation of hydrophobic residues towards the lipid/water interface. It is generally assumed that a substantiated hydrophobic content is required to interact with the core of the membrane and to destabilize it. In the absence of any hydrophobic residues, insertion of side-chains that favor guanidinium moiety to phosphate interaction is another mechanism of destabilization. The relevance of the arginine–phosphate interactions has been highlighted in several reports (Herce and Garcia, 2007a,b).

An important difference between cell-penetrating peptides and antimicrobial peptides is the lack of hydrophobic residues in the former case. Our data show that despite being charged and highly hydrophilic, peptides composed entirely of arginine amino acids are able to destabilize and permeabilize the lipid bilayer.

## References


Bechinger, B., Ruysschaert, J.M., Goormaghtigh, E., 1999. Membrane helix orientation from linear dichroism of infrared attenuated total reflection spectra. Biophys. J. 76 (1 (Pt 1)), 552–563.

Berendsen, H.J.C., Postma, J.P.M., Van Gunsteren, W.F., Hermans, J., 1981. Interaction models for water in relation to protein hydration. In: Reidel, Dordrecht (Eds.), Intermolecular Forces, pp. 331–342.

Berendsen, H.J.C., Postma, J.P.M., van Gunsterren, W.F., DiNola, A., Haak, J.R., 1984. Molecular dynamics with coupling to an external bath. J. Chem. Phys. 81 (8), 3684–3690.

Binder, H., Lindblom, G., 2003. Charge-dependent translocation of the Trojan peptide penetratin across lipid membranes. Biophys. J. 85 (2), 982–995.

Casal, H.L., Mantsch, H.H., 1984. Polymorphic phase behaviour of phospholipid membranes studied by infrared spectroscopy. Biochim. Biophys. Acta 779 (4), 381–401.

Essman, U., Perela, L., Berkowitz, M.L., Darden, T., Lee, H., Pedersen, L.G., 1995. A smooth particle mesh Ewald method. J. Chem. Phys. 103, 8577–8592.

Feenstra, K.A., Hess, B., Berendsen, H.J.C., 1999. Improving efficiency of large time-scale molecular dynamics simulations of hydrogen-rich systems. J. Comput. Chem. 20, 786–798.

Freites, J.A., Tobias, D.J., von, H.G., White, S.H., 2005. Interface connections of a transmembrane voltage sensor. Proc. Natl. Acad. Sci. U. S. A. 102 (42), 15059–15064.

Futaki, S., 2006. Oligoarginine vectors for intracellular delivery: design and cellular-uptake mechanisms. Biopolymers 84 (3), 241–249.

Goormaghtigh, E., Ruysschaert, J.M., Raussens, V., 2006. Evaluation of the information content in infrared spectra for protein secondary structure determination. Biophys. J. 90 (8), 2946–2957.

Grimard, V., Vigano, C., Margolles, A., Wattiez, R., van Veen, H.W., Konings, W.N., Ruysschaert, J.M., Goormaghtigh, E., 2001. Structure and dynamics of the membrane-embedded domain of LmrA investigated by coupling polarized ATR-FTIR spectroscopy and (1)H/(2)H exchange. Biochemistry 40 (39), 11876–11886.

Heerklotz, H., Seelig, J., 2007. Leakage and lysis of lipid membranes induced by the lipopeptide surfactin. Eur. Biophys. J. 36 (4–5), 305–314.

Henriques, S.T., Costa, J., Castanho, M.A., 2005. Translocation of beta-galactosidase mediated by the cell-penetrating peptide pep-1 into lipid vesicles and human HeLa cells is driven by membrane electrostatic potential. Biochemistry 44 (30), 10189–10198.

Herce, H.D., Garcia, A.E., 2007a. Cell penetrating peptides: how do they do it? J. Biol. Phys. 33 (5–6), 345–356.

Herce, H.D., Garcia, A.E., 2007b. Molecular dynamics simulations suggest a mechanism for translocation of the HIV-1 TAT peptide across lipid membranes. Proc. Natl. Acad. Sci. U. S. A. 104 (52), 20805–20810.

Hess, B., Bekker, H., Berendsen, H.J., Fraaije, J., 1997. LINCS: a linear constraint solver for molecular simulations. J. Comput. Chem. 18 (12), 1463–1472.

Kabsch, W., Sander, C., 1983. Dictionary of protein secondary structure: pattern recognition of hydrogen-bonded and geometrical features. Biopolymers 22 (12), 2577–2637.

Lensink, M.F., Christiaens, B., Vandekerckhove, J., Prochiantz, A., Rosseneu, M., 2005. Penetratin–membrane association: W48/R52/W56 shield the peptide from the aqueous phase. Biophys. J. 88 (2), 939–952.

MacCallum, J.L., Bennett, W.F., Tieleman, D.P., 2008. Distribution of amino acids in a lipid bilayer from computer simulations. Biophys. J. 94 (9), 3393–3404.

MacCallum, J.L., Bennett, W.F., Tieleman, D.P., 2011. Transfer of arginine into lipid bilayers is nonadditive. Biophys. J. 101 (1), 110–117.

Mitchell, D.J., Kim, D.T., Steinman, L., Fathman, C.G., Rothbard, J.B., 2000. Polyarginine enters cells more efficiently than other polycationic homopolymers. J. Pept. Res. 56 (5), 318–325.

Miyamoto, S., Kollman, P.A., 1992. Settle: an analytical version of the SHAKE and RATTLE algorithm for rigid water models. J. Comput. Chem. 13, 952–962.

Oberg, K.A., Ruysschaert, J.M., Goormaghtigh, E., 2004. The optimization of protein secondary structure determination with infrared and circular dichroism spectra. Eur. J. Biochem. 271 (14), 2937–2948.

Richard, J.P., Melikov, K., Brooks, H., Prevot, P., Lebleu, B., Chernomordik, L.V., 2005. Cellular uptake of unconjugated TAT peptide involves clathrin-dependent endocytosis and heparan sulfate receptors. J. Biol. Chem. 280 (15), 15300–15306.

Rothbard, J.B., Kreider, E., VanDeusen, C.L., Wright, L., Wylie, B.L., Wender, P.A., 2002. Arginine-rich molecular transporters for drug delivery: role of backbone spacing in cellular uptake. J. Med. Chem. 45 (17), 3612–3618.

Rouser, G., Siakotos, A.N., Fleischer, S., 1966. Quantitative analysis of phospholipids by thin-layer chromatography and phosphorus analysis of spots. Lipids 1 (1), 85–86.

Sakai, N., Takeuchi, T., Futaki, S., Matile, S., 2005. Direct observation of anion-mediated translocation of fluorescent oligoarginine carriers into and across bulk liquid and anionic bilayer membranes. Chembiochem 6 (1), 114–122.

Scheirlinckx, F., Raussens, V., Ruysschaert, J.M., Goormaghtigh, E., 2004. Conformational changes in gastric $H^+/K^+$-ATPase monitored by difference Fourier-transform infrared spectroscopy and hydrogen/deuterium exchange. Biochem. J. 382 (Pt 1), 121–129.

Schwieger, C., Blume, A., 2009. Interaction of poly(L-arginine) with negatively charged DPPG membranes: calorimetric and monolayer studies. Biomacromolecules 10 (8), 2152–2161.

Tang, M., Waring, A.J., Hong, M., 2007. Phosphate-mediated arginine insertion into lipid membranes and pore formation by a cationic membrane peptide from solid-state NMR. J. Am. Chem. Soc. 129 (37), 11438–11446.

Tieleman, D.P., Sansom, M.S., Berendsen, H.J., 1999. Alamethicin helices in a bilayer and in solution: molecular dynamics simulations. Biophys. J. 76 (1 (Pt 1)), 40–49.

Tung, C.H., Weissleder, R., 2003. Arginine containing peptides as delivery vectors. Adv. Drug Deliv. Rev. 55 (2), 281–294.

Van Der Spoel, D., Lindahl, E., Hess, B., Groenhof, G., Mark, A.E., Berendsen, H.J., 2005. GROMACS: fast, flexible, and free. J. Comput. Chem. 26 (16), 1701–1718.

van Gunsteren, W.F., 1996. Biomolecular simulation. In: The GROMOS96 Manual and User Guide. Hochschulverlag AG an der ETH Zürich, Zürich, Switzerland.

Venyaminov, S.Y., Kalnin, N.N., 1990. Quantitative IR spectrophotometry of peptide compounds in water ($H_2O$) solutions. I. Spectral parameters of amino acid residue absorption bands. Biopolymers 30 (13–14), 1243–1257.

Vigano, C., Manciu, L., Buyse, F., Goormaghtigh, E., Ruysschaert, J.M., 2000a. Attenuated total reflection IR spectroscopy as a tool to investigate the structure, orientation and tertiary structure changes in peptides and membrane proteins. Biopolymers 55 (5), 373–380.

Vigano, C., Margolles, A., van Veen, H.W., Konings, W.N., Ruysschaert, J.M., 2000b. Secondary and tertiary structure changes of reconstituted LmrA induced by nucleotide binding or hydrolysis. A Fourier transform attenuated total reflection infrared spectroscopy and tryptophan fluorescence quenching analysis. J. Biol. Chem. 275 (15), 10962–10967.

Wadia, J.S., Stan, R.V., Dowdy, S.F., 2004. Transducible TAT-HA fusogenic peptide enhances escape of TAT-fusion proteins after lipid raft macropinocytosis. Nat. Med. 10 (3), 310–315.

Wender, P.A., Rothbard, J.B., Jessop, T.C., Kreider, E.L., Wylie, B.L., 2002. Oligocarbamate molecular transporters: design, synthesis, and biological evaluation of a new class of transporters for drug delivery. J. Am. Chem. Soc. 124 (45), 13382–13383.

Wolpert, M., Hellwig, P., 2006. Infrared spectra and molar absorption coefficients of the 20 alpha amino acids in aqueous solutions in the spectral range from 1800 to 500 $cm^{-1}$. Spectrochim. Acta A: Mol. Biomol. Spectrosc. 64 (4), 987–1001.